1703

On the Electronic Structure of [1Fe] Fe−S Complexes from Anionic Photoelectron Spectroscopy

Xin Yang, Xue-Bin Wang, You-Jun Fu, and Lai-Sheng Wang*

Department of Physics, Washington State University, 2710 University Drive, Richland, Washington 99352, and W.R. Wiley Environmental Molecular Sciences Laboratory, MS K8-88, P.O. Box 999, Pacific Northwest National Laboratory, Richland, Washington 99352

The electronic structure of a series of Fe−S complexes, $Fe(SCN)_3^-$, $Fe(SCN)_4^-$, $Na^+[Fe(SCN)_4^{2-}]$, $Fe(SCH_3)_3^-$, $Fe(SCH_3)_4^-$, $Na^+[Fe(S_2\text{-}o\text{-xyl})_2^{2-}]$, and $Fe(S_2\text{-}o\text{-xyl})_2^-$ (where $S_2\text{-}o\text{-xyl}$ = o-xylene-α,α'-dithiolate), was investigated in the gas phase using photodetachment photoelectron spectroscopy. Spectral features due to detachment from metal d orbitals or ligand orbitals were distinguished by comparing with the spectrum of a d^0 complex, $Sc(SCN)_4^-$. A weak threshold feature was observed in the spectra of all ferrous complexes due to detachment of the minority spin Fe $3d$ electron [Fe^{II} $(3d^6) \rightarrow Fe^{III}$ $(3d^5)$]. The spin majority Fe $3d$ electron signals were observed at much higher binding energies, revealing directly the "inverted level scheme" for these [1Fe] Fe−S complexes based on previous spin polarized calculations. The "inverted level scheme" is shown to be a general feature of the electronic structures of the [1Fe] Fe−S complexes, independent of the oxidation state and coordination number. Information about the gas-phase redox potentials and reorganization energies upon oxidation of the ferrous complexes is obtained from the adiabatic and vertical detachment energies of the minority Fe $3d$ electron.

Introduction

Iron−sulfur proteins are found in all forms of life. Rubredoxin is the simplest iron−sulfur protein, containing a single Fe at its active site coordinated tetrahedrally with four cysteine sulfur atoms,[1] as shown schematically in Figure 1. It exists in both ferric [Fe(III)] and ferrous [Fe(II)] oxidation states and serves as an electron-transfer agent in cells.[2,3] The redox potential of this redox couple is in the range of −95 to 60 mV,[4] much lower than the aqueous Fe^{3+}/Fe^{2+} couple (+770 mV), indicating that there is an intrinsic stabilization of the ferric relative to the ferrous ion due to the thiolate ligands. A detailed understanding of the electronic structure of the complexes involved in the redox couple is essential to elucidate their electron-transfer functions and other chemical properties. Compared with the native Fe−S clusters in proteins, synthetic analogues can be studied more straightforwardly and can provide more detailed insight into the properties of the active site itself. Indeed, many model systems of the [1Fe] active site in rubredoxin have been synthesized since the early 1970s by replacing the cysteine chains with simple thiolate ligands.[5−18] Various spectroscopic methods, such as X-ray diffraction,[19,20] resonance Raman spectroscopy,[18] and Mossbauer spectroscopy,[11] have been used to investigate the active site of the [1Fe] analogue complexes and have shown that most of these analogues have a high-spin tetrahedral [FeS₄] unit and can be considered as reasonable stereochemical representations of the [1Fe] active site in rubredoxin.

There have also been numerous theoretical studies on the [1Fe] Fe−S complexes.[21−27] Two different types of first-principle calculations have been applied to the single iron Fe−S clusters: unrestricted Hartree−Fock methods on $Fe(SH)_4^{1-/2-}$ and $Fe(SCH_3)_4^{1-/2-}$,[21,22] and spin-polarized Xα-scattered wave
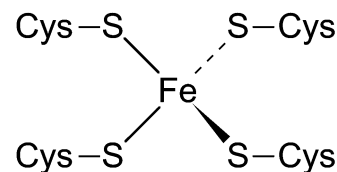

Figure 1. Schematic structure of the [1Fe] site in rubredoxin.

methods on FeS_4^{6-}, FeS_4^{5-}, $Fe(SH)_4^-$, and $Fe(SCH_3)_4^{1-/2-}$.[23−25] However the results were not consistent. The unrestricted Hartree−Fock results are similar to standard ligand field models (derived from low spin systems) where all occupied metal levels lie above all occupied ligand levels and the lowest unoccupied levels are also metal in character. When the molecular orbitals (MOs) are optimized in the spin-polarized self-consistent field (SCF) procedure, the spin-up (α) and spin-down (β) electrons are treated separately. For a high-spin transition metal site in the presence of a weak ligand field, such as S, the majority spin electrons are stabilized in energy, while the corresponding minority spin electrons are destabilized. In the oxidized (ferric) complexes, there is a 4−5 eV splitting between the occupied spin-up Fe $3d$ orbitals and the unoccupied spin-down Fe $3d$ orbitals. The mainly S-based Fe−S bonding and antibonding and S $3p$ nonbonding levels lie between the predominantly spin-polarized Fe $3d$ levels,[26,27] as schematically shown in Figure 2. In the reduced (ferrous) complexes, the same level pattern applies, with the extra electron entering the Fe $3d$ (β) highest occupied molecular orbital (HOMO). This MO pattern is called the "inverted level scheme" to distinguish it from the normal ligand field model.[26,27]

This "inverted level scheme" agrees well with photoelectron and X-ray absorption spectroscopy experiments for the ferric complexes, $Fe(SR)_4^-$.[28−30] However, the energy level scheme of the reduced compounds remains controversial. Theoretical
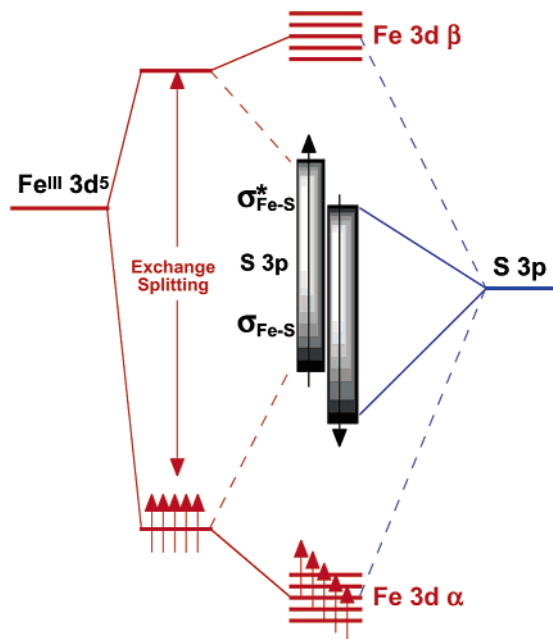
Figure 2. Schematic energy level diagram for ferric $[Fe(SR)_4]^{1-}$ complexes according to spin polarization calculations.

calculations show that the differences in the orbital energy diagrams between the oxidized and reduced clusters are minor.[23,25] The presence of the extra electron in the reduced complexes has only a small effect on the orbital energies, aside from a uniform upward shift. However, single-crystal spectroscopic studies of $Fe(SR)_4^{2-}$ $[R = 2\text{-}(Ph)C_6H_4]$ suggest a picture consistent with the standard spin restricted ligand field model and a large electronic relaxation upon reduction.[15]

Three-coordinate Fe^{II} thiolate complexes have aroused much interest recently as models for the trigonal sites of the $MoFe_7S_9$ cofactor of nitrogenase.[31] Analyses of Q-band ENDOR data[32] and Mossbauer data[33] suggest that the majority of the trigonal sites are high-spin ferrous centers. The synthesis and structure of a three-coordinate Fe^{II} model complex, $Fe(SR)_3^-$ $(R = C_6H_2$-$2,4,6\text{-}t\text{Bu}_3)$ have been published.[34] The Fe site exhibits a slightly distorted planar geometry with idealized C_{3h} symmetry. Recently, a Mossbauer investigation has been carried out on this analogue complex.[35]

Gas-phase photodetachment photoelectron spectroscopy (PES) is a valuable tool to study the electronic structure and chemical bonding of isolated molecules or inorganic complexes without the perturbation encountered in the condensed phase environments. We have recently developed an experimental technique that couples an electrospray ionization (ESI) source with a magnetic-bottle photoelectron spectrometer.[36] ESI is a versatile technique, allowing ionic species in solution samples to be transported into the gas phase. Our recent research has shown that the ESI–PES technique is ideal for the investigation of multiply charged anions in the gas phase,[37] as well as anionic metal-complexes commonly present in solution.[38–42] Using this technique, we have reported a preliminary study of a series of [1Fe]-complexes involved in the Fe^{II}/Fe^{III} redox couple, with emphasis on the determination of the intramolecular reorganization energies from PES data of the Fe^{II} complexes.[40]

In the current paper, we present a detailed PES study of the [1Fe]-complexes, aiming at elucidating their electronic structures. PES spectra were obtained for $Fe(SCN)_3^-$, $Fe(SCN)_4^-$, $Na^+[Fe(SCN)_4^{2-}]$, $Fe(SCH_3)_3^-$, $Fe(SCH_3)_4^-$, $Na^+[Fe(S_2\text{-}o\text{-}xyl)_2^{2-}]$, and $Fe(S_2\text{-}o\text{-}xyl)_2^-$ (where $S_2\text{-}o\text{-}xyl = o$-xylene-$\alpha,\alpha'$-dithiolate) at three photon energies: 266, 193, and 157 nm. The

spectral patterns of these complexes agree well with previous spin-polarized calculations. The similarity between the spectra of the ferrous and ferric complexes suggest that the "inverted level scheme" should be a general feature for describing the electronic structure of the high-spin [1Fe] Fe—S complexes regardless of the oxidation state and coordination number.

Experimental Section

Sample Preparation. The $Fe(SCN)_{3/4}^-$ and $Fe(SCH_3)_{3/4}^-$ sample solutions were prepared by adding $FeCl_2$ and $NaSCN$ or $NaSCH_3$ at a molar ratio of 1:4 in pure acetonitrile (or methanol) at 0 °C. The $[Fe^{II/III}(S_2\text{-}o\text{-}xyl)_2]^{2-/1-}$ sample solution was prepared by adding sodium ethoxide (1.73 M in ethanol) in a suspension of $FeCl_2$ and 1,2-benzenedimethanethiol (1:2 volume ratio) in pure ethanol at 0 °C. The concentration of the target anion in each solution was about 10^{-3} M. All sample manipulations were performed under a pure N_2 atmosphere and all solvents were carefully degassed prior to use. Because the samples were prepared in a reduction atmosphere, the synthetic analogues were all ferrous complexes in the solution. When the samples were sprayed in ambient atmosphere, however, the ferrous complexes could be oxidized in the ESI source. Thus both ferrous and ferric species were observed in the mass spectra.

Photodetachment Photoelectron Spectroscopy. Details of the ESI–PES apparatus were published elsewhere.[36] Only a brief description of the experimental procedure is given here. The sample solutions were sprayed through a 0.01 mm diameter syringe needle biased at -2.2 kV in a N_2 (for reduced complexes) or ambient atmosphere (for oxidized complexes). Negatively charged ions emerging from a desolvation capillary were guided by a radio frequency quadrupole ion-guide into an ion trap, where the ions were accumulated for 0.1 s before being pushed into the extraction zone of a time-of-flight mass spectrometer. The anions of interest were mass-selected and decelerated before being intercepted by a laser beam in the detachment zone of the magnetic-bottle photoelectron analyzer. For the current study, three photon energies were used for photodetachment: 266 nm (4.661 eV) from a Q-switched Nd: YAG laser, and 193 nm (6.424 eV) and 157 nm (7.866 eV) from an excimer laser. Photoelectrons were collected at nearly 100% efficiency by the magnetic-bottle and analyzed in a 4 m long time-of-flight tube. Photoelectron time-of-flight spectra were collected and then converted to kinetic energy spectra, calibrated by the known spectra of I^- and O^-. The binding energy spectra were obtained by subtracting the kinetic energy spectra from the corresponding photon energies. The energy resolution ($\Delta E/E$) was about 2%, i.e., 10 meV (fwhm) for $\sim$0.5 eV electrons, as measured from the spectrum of I^- at 355 nm.

Results

Photoelectron Spectra of $Fe(SCN)_3^-$, $Na^+[Fe(SCN)_4^{2-}]$, $Fe(SCN)_4^-$, and $Sc(SCN)_4^-$ Complexes. For the SCN^- complexes, both the three-coordinate ferrous $Fe(SCN)_3^-$ and the four-coordinate ferric $Fe(SCN)_4^-$ anions were observed from our ESI source. The isolated tetrahedral ferrous $Fe(SCN)_4^{2-}$ dianion was not observed because it is not expected to be stable in the gas phase due to the strong intramolecular coulomb repulsion. However, it can be stabilized by a cation and was indeed observed as a Na^+ ion pair. Figure 3 shows the PES spectra at 157 nm of $Fe(SCN)_3^-$, $Na^+[Fe(SCN)_4^{2-}]$, and $Fe(SCN)_4^-$, compared with the spectrum of $Sc(SCN)_4^-$, which formally has no $3d$ electron on the metal center.

Electronic Structure of [1Fe] Fe−S Complexes

J. Phys. Chem. A, Vol. 107, No. 11, 2003 **1705**
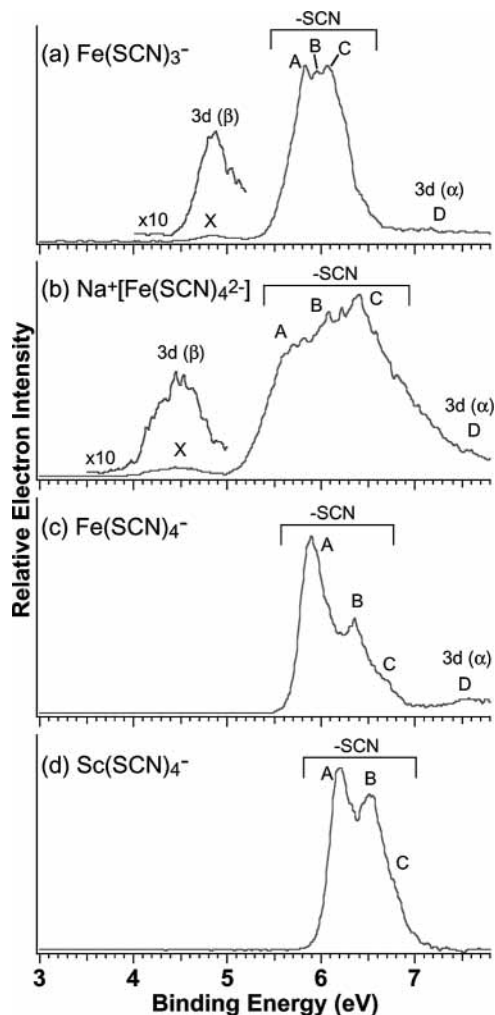
Figure 3. Photoelectron spectra of (a) $Fe(SCN)_3^-$, (b) $Na^+[Fe(SCN)_4^{2-}]$, (c) $Fe(SCN)_4^-$, and (d) $Sc(SCN)_4^-$ at 157 nm.

The spectra of $Fe(SCN)_3^-$ (Figure 3a) is dominated by a strong band centered at around 6 eV with three discernible fine features (A, B, C). A very weak but well-defined feature (X) at lower binding energies is observed at a vertical detachment energy (VDE) of 4.96 eV. The energy gap between the features X and A is ∼0.9 eV. At higher binding energies (>6.5 eV), weak and continuous signals were observed (D). The intensity of this flat tail is similar to that of the threshold peak (X). The spectrum of $Na^+[Fe(SCN)_4^{2-}]$ (Figure 3b) is similar to that of $Fe(SCN)_3^-$, but much broader. Again, a very weak threshold band (X) was observed at a VDE of 4.56 eV, followed by a large energy gap (∼1 eV) and a group of intense bands (A, B, C), which were likely to contain numerous overlapping transitions. On the high binding energy side, weak signals (D) were still present.

The spectrum of $Fe(SCN)_4^-$ (Figure 3c) seems to be relatively simple with very high electron binding energies. The weak low binding energy features observed in the ferrous complex is absent in the spectrum of the ferric complex. The threshold feature of $Fe(SCN)_4^-$ is very intense with a VDE of 5.88 eV, following which a well resolved band (B) was observed at a VDE of 6.36 eV. On the higher binding energy side, another weak feature is discernible (C). At very high binding energies (>7 eV), weak signals (D) were also present, similar to those observed in the spectrum of $Fe(SCN)_3^-$ (Figure 3a). The spectrum of $Sc(SCN)_4^-$ (Figure 3d) is the simplest with two well-resolved bands (A and B) and a shoulder (C) on the high

energy side. It shows some similarity to that of $Fe(SCN)_4^-$, but has very high binding energies with a VDE for the A band at 6.20 eV. Unlike the spectrum of $Fe(SCN)_4^-$, however, the high binding energy side (>7.2 eV) of the $Sc(SCN)_4^-$ spectrum is very clean and reaches to the baseline.

Photoelectron Spectra of $Fe(SCH_3)_3^-$ and $Fe(SCH_3)_4^-$ Complexes. Figure 4 shows the PES spectra of $Fe(SCH_3)_3^-$ and $Fe(SCH_3)_4^-$ at three different photon energies. Analogous to $Fe(SCN)_4^{2-}$, the isolated tetracoordinate ferrous $Fe(SCH_3)_4^{2-}$ dianion is not expected to be stable. But we were not able to observe the Na^+ stabilized complex, $Na^+[Fe(SCH_3)_4^{2-}]$. For the tri-coordinate ferrous complex (Figure 4a), a well resolved and relatively weak threshold peak (X) at a VDE of 3.08 eV was observed. Following an energy gap of ∼0.8 eV, a group of intense and broad bands between 3.5 and 5.5 eV is revealed in the high photon energy spectra. The spectrum in this energy range likely contains numerous overlapping features, but three (A, B, C) are tentatively identified for later discussions. At even higher binding energies (>5.5 eV) in the 157 nm spectrum, two well separated peaks are observed (D and E), but significant signals exist between the two main peaks.

The weak threshold peak observed in the spectra of the ferrous complex is absent in the PES spectra of the tetracoordinate ferric complex, $Fe(SCH_3)_4^-$, as shown in Figure 4b. Remarkably, the overall spectral features of the ferric complex are rather similar to those of the ferrous complex beside the weak threshold feature in the latter. The relative intensity of the A band was enhanced in the spectra of the ferric complex, but the features in the higher binding energy part (D to E) appear identical in the two systems.

Photoelectron Spectra of $Na^+[Fe(S_2\text{-}o\text{-xyl})_2^{2-}]$ and $Fe(S_2\text{-}o\text{-xyl})_2^-$ Complexes. For the bidentate ligand ($=S_2\text{-}o\text{-xyl}$), we were able to observe the ferrous dianion $Fe(S_2\text{-}o\text{-xyl})_2^{2-}$ stabilized by a Na^+ cation. Figure 5 shows the PES spectra of $Na^+[Fe(S_2\text{-}o\text{-xyl})_2^{2-}]$ and the ferric complex $Fe(S_2\text{-}o\text{-xyl})_2^-$ at three photon energies. Again, a weak threshold feature (X) was observed in the spectra of the ferrous complex (Figure 5a), but not in those of the ferric complex (Figure 5b). The VDE of the weak threshold peak in the spectra of the ferrous complex is 2.60 eV. The energy gap between the X and A features is ∼0.9 eV, similar to those observed in the ferrous complexes of −SCN and −SCH_3. The overall spectral patterns of the ferrous and ferric complexes of the bidentate ligand are similar to those of the ferric and ferrous complexes of −SCH_3. The only significant difference is band D, which appeared to be much stronger in the dithiol complexes.

VDEs and ADEs. The ADEs of the threshold peaks represent the electron affinities of the neutral species in each case and are related to the redox properties of the metal complexes in solution. The ADEs were determined from the 193 nm spectra[40] for the −SCN complexes and the 266 nm spectra for the −SCH_3 and =$S_2\text{-}o\text{-xyl}$ complexes. Whereas the VDE could be measured straightforwardly from the peak maximum, the ADE was estimated by drawing a straight line along the leading edge of the threshold band and then adding a constant to the intersection with the binding energy axis to take into account the resolution and a finite thermal broadening. Since the resolution depends on the binding energies and the photon energies, the constant added in each case is different. The ADEs measured from the lower photon energy spectra were more accurate due to the enhanced resolution. The ADE represents the 0−0 transition from the anion to the neutral. In cases of large geometry changes, the Franck−Condon factor for the 0−0 transition may be too small to be observed in the PES spectra, so that the ADEs obtained from the above extrapolation procedure would only
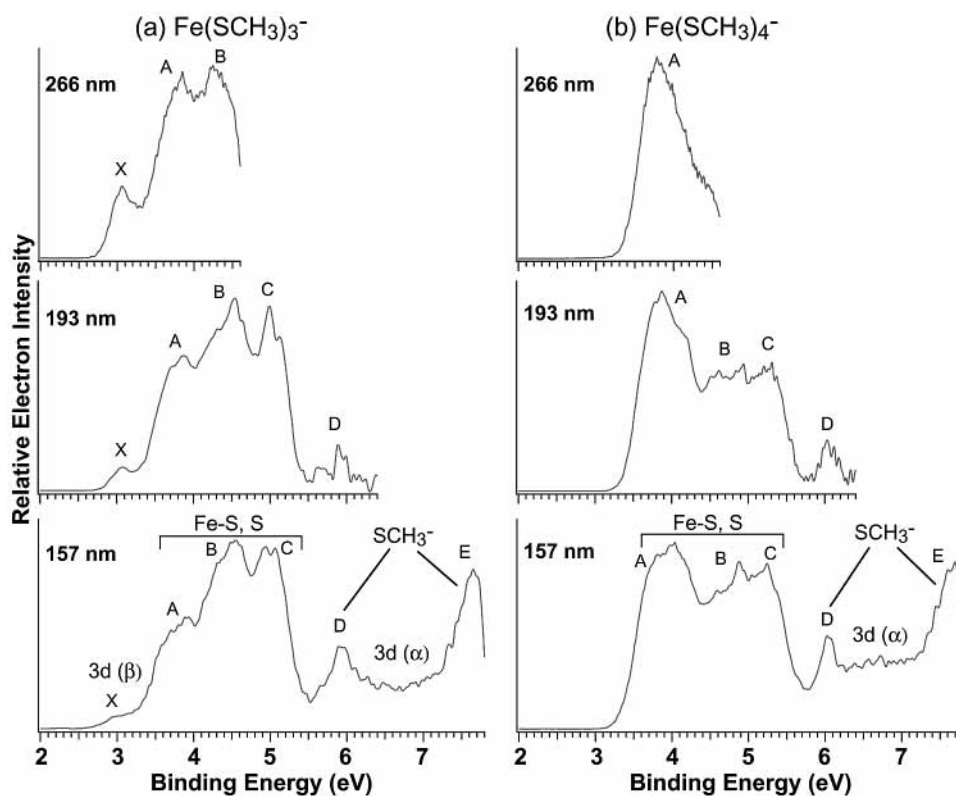
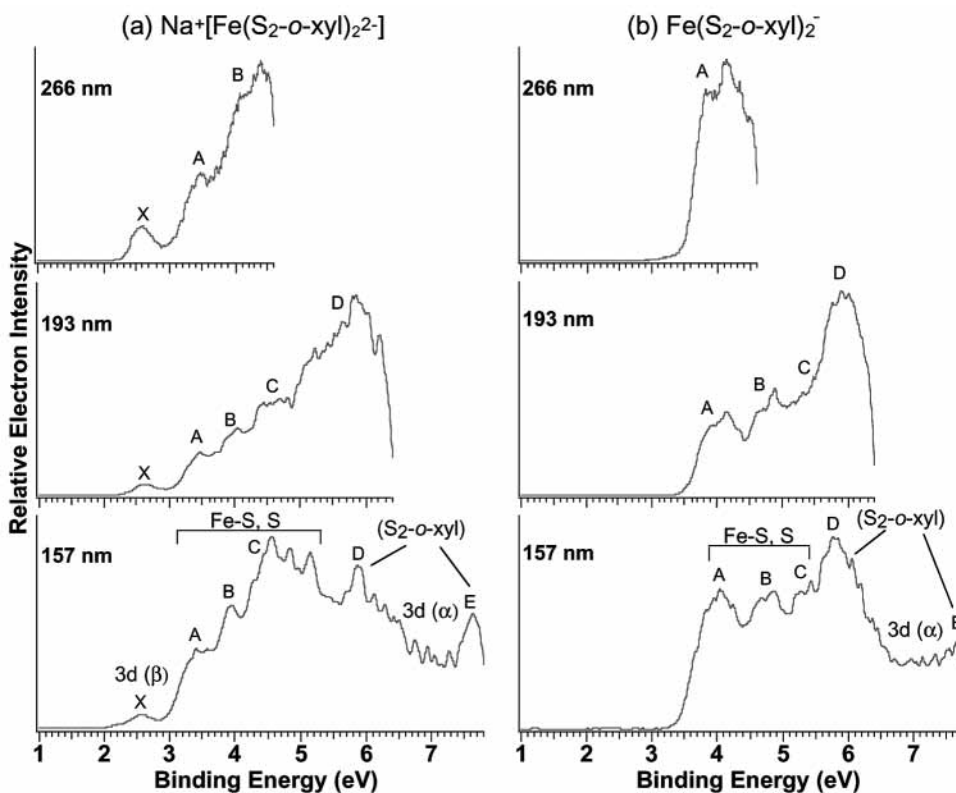**Figure 4.** Photoelectron spectra of (a) $Fe(SCH_3)_3^-$ and (b) $Fe(SCH_3)_4^-$ at 266, 193, and 157 nm.

Figure 5. Photoelectron spectra of (a) $Na^+[Fe(S_2\text{-}o\text{-xyl})_2^{2-}]$ and (b) $Fe(S_2\text{-}o\text{-xyl})_2^-$ at 266, 193, and 157 nm.

yield the upper limits. However, as will be shown below, the electrons removed for the threshold peaks in the PES spectra of the current set of complexes all involve nonbonding electrons, which may not cause too great a geometrical change to render unobservable Franck−Condon factors for the 0−0 transitions.

Thus, the ADEs obtained currently should represent reasonable estimates for the true ADEs, which could only be measured accurately with vibrationally resolved PES data. The ADE and VDE of the threshold peak of each complex are listed in Table 1. The VDEs of all observed features are listed in Table 2.

Electronic Structure of [1Fe] Fe−S Complexes

J. Phys. Chem. A, Vol. 107, No. 11, 2003 **1707**

TABLE 1: Measured Adiabatic (ADE) and Vertical (VDE) Detachment Energies for the Threshold Peaks, Reorganization Energies (VDE-ADE), and (A−X) Energy Gaps (ΔE) in eV

	ADE[a]	VDE[b]	VDE-ADE	ΔE^c
$Fe(SCN)_3^-$	4.64 (5)	4.96 (8)	0.32	0.9
$Na^+[Fe(SCN)_4^{2-}]$	4.12 (5)	4.56 (8)	0.44	1.0
$Fe(SCN)_4^-$	5.70 (5)	5.88 (5)	0.18	
$Sc(SCN)_4^-$	5.98 (5)	6.20 (5)	0.22	
$Fe(SCH_3)_3^-$	2.80 (6)	3.08 (5)	0.28	0.8
$Fe(SCH_3)_4^-$	3.38 (5)	3.82 (8)	0.44	
$Na^+[Fe(S_2\text{-}o\text{-xyl})_2^{2-}]$	2.30 (5)	2.60 (5)	0.30	0.9
$Fe(S_2\text{-}o\text{-xyl})_2^-$	3.49 (5)	3.90 (8)	0.41	

a Adiabatic electron affinities of the corresponding neutral species. The numbers in the parentheses represent the uncertainties in the last digit. *b* The VDE was measured from the peak maximum. The numbers in the parentheses represent the uncertainties in the last digit. *c* Estimated from the VDEs of the first (X) and second (A) detachment features from the respective PES spectra.

Discussion

The PES features shown in Figures 3−5 represent transitions from the ground state of the anions to the ground and excited states of the corresponding neutral molecules. Within the single-particle approximation, these PES features can be alternatively viewed as removing electrons from the occupied molecular orbitals of the anions. Therefore, unlike other various experimental methods based on electronic transitions from occupied MOs to empty or partially empty MOs, PES provides a direct map of the occupied MOs. Furthermore, for anions involved in electron transfer reactions (such as the ferrous complexes), PES data directly yield the intrinsic oxidation energies and intramolecular reorganization energies in the gas phase since photodetachment is equivalent to an oxidation process in solution except that the solvation effect is absent.[40]

Overview of the Electronic Structures of the [1Fe] Ferric and Ferrous Complexes. The iron−sulfur proteins and synthetic analogues are challenging electronic systems for quantum mechanical methods because spin polarization and spin couplings are essential features of these complexes.[26,27] Standard approaches of ab initio quantum chemistry, starting from a spin-restricted picture, are poorly adapted to problems involving high spin transition metal centers.[43] In the spin-restricted SCF calculations for $Fe^{III}S_4^{5-}$ and $Fe^{III}(SR)_4^-$ (R = H, CH$_3$),[21,22,24] the highest occupied orbitals are five-half-filled Fe−S antibonding orbitals with mainly Fe 3d characters. The lowest energy member of these five metal-based orbitals is primarily d_{z^2}. Upon reduction, the extra electron is added to this MO in the ferrous complexes.

As shown in Figure 2, spin-polarized calculations using SCF-Xα-SW methods produced marked changes in the MO levels of the Fe−S complexes.[24,25] The strong exchange interactions split the Fe 3d levels into a set of spin-up (α) and a set of spin-down (β) levels. The majority spin levels (α) are considerably

stabilized in energy with the primarily ligand-based levels between the Fe 3d minority and majority levels, resulting in the so-called "inverted level scheme". Thus, in the ferric complexes, the HOMO becomes ligand-based orbitals. In the ferrous complexes, the extra electron enters the high-energy Fe 3d minority level. In the following discussion, we show that our PES data are in qualitative agreement with this energy scheme.

$Fe(SCN)_3^-$, $Na^+[Fe(SCN)_4^{2-}]$, $Fe(SCN)_4^-$, and $Sc(SCN)_4^-$. The electron configuration of the central metal atom in the $Sc(SCN)_4^-$ complex is d^0 and has no occupied 3d MOs. The PES spectrum of this complex provides an excellent reference to assign the 3d vs ligand features in the PES spectra of the corresponding Fe−SCN complexes. The spectrum of $Sc(SCN)_4^-$ (Figure 3d) contains three strong features in a relatively narrow energy range between 6 and 7 eV. These features should be entirely due to detachment from ligand-based MOs. The three intense low binding energy features in the spectrum of $Fe(SCN)_4^-$ are very similar to those of the $Sc(SCN)_4^-$ spectrum and they should be due to the −SCN ligands accordingly. This observation suggests that indeed the HOMO of this ferric complex is a ligand-based MO. The weak high binding energy signals (D), which are absent in the spectrum of $Sc(SCN)_4^-$, are assigned to be due to detachment from the Fe 3d α levels. This assignment is in qualitative agreement with the inverted level scheme depicted in Figure 2.

For the two ferrous complexes, the extra electron occupies one Fe 3d β level, resulting in the weak threshold feature (X). The high binding energy features (A−D) in the spectrum of the tri-coordinate $Fe(SCN)_3^-$ complex are remarkably similar to those of the tetracoordinate $Fe(SCN)_4^-$, and are assigned similarly. Thus, we see that not only the inverted energy scheme applies equally to the ferric and the ferrous complexes, but it is also independent of the number of ligands. The spectral pattern of the $Na^+[Fe(SCN)_4^{2-}]$ ferrous complex is similar to that of the ferrous $Fe(SCN)_3^-$, but much broadened, probably due to the symmetry-breaking effect of the Na^+ cation or large geometry changes upon electron detachment. The latter may have a large contribution because of the significantly altered electrostatic environment for the Na^+ cation upon electron detachment from the $Na^+[Fe(SCN)_4^{2-}]$ complex.

$Fe^{II/III}(SCH_3)_{3/4}^-$ and $Fe^{II/III}(S_2\text{-}o\text{-xyl})_2^{2-/1-}$ Complexes. The spectral similarity between $Fe^{II/III}(SCH_3)_{3/4}^-$ (Figure 4) is analogous to that between $Fe^{II/III}(SCN)_{3/4}^-$. The more complicated spectral patterns observed in the −SCH$_3$ complexes compared to those of the −SCN complexes are due to the more complicated valence MO levels of the −SCH$_3$ ligands. From Figure 3, we see that detachment cross sections for the Fe 3d electrons are relatively low within our photon energy range. For the ferrous $Fe(SCH_3)_3^-$ complex, the weak threshold feature (X) is assigned to be due to detachment of the Fe 3d β electron, similar to that in the $Fe(SCN)_3^-$ spectrum. The intense features (A−E) are assigned to be from detachment from the ligands.

TABLE 2: Measured Vertical Detachment Energies (VDE) (in eV) for All Observed Features[a]

	X	A	B	C	D	E
$Fe(SCN)_3^-$	4.96 (8)	5.83 (5)	5.95 (5)	6.07 (6)		
$Na^+[Fe(SCN)_4^{2-}]$	4.56 (8)	5.60 (10)	6.08 (10)	6.41 (10)		
$Fe(SCN)_4^-$		5.88 (5)	6.36 (5)	∼6.7		
$Sc(SCN)_4^-$		6.20 (5)	6.52 (5)	∼6.8		
$Fe(SCH_3)_3^-$	3.08 (5)	3.85 (10)	∼4.5	∼5	5.9 (1)	>7.5
$Fe(SCH_3)_4^-$		3.82 (8)	∼4.5−4.9	∼5.2	6.0 (1)	>7.5
$Na^+[Fe(S_2\text{-}o\text{-xyl})_2^{2-}]$	2.60 (5)	3.46 (8)	3.96 (10)	4.3−5.3	5.9 (1)	>7.5
$Fe(S_2\text{-}o\text{-xyl})_2^-$		3.90 (8)	4.88 (10)	∼5.3	5.9 (1)	>7.5

a The numbers in the parentheses represent the uncertainties in the last digit.

The weak signals between features D and E are assigned to be from detachment of the Fe $3d$ α electrons tentatively. The spectra of the ferric $Fe(SCH_3)_4^-$ complex are assigned similarly. These assignments are again consistent with the inverted energy scheme shown in Figure 2. The spectra of the $=S_2$-o-xyl bidentate complexes are similar to those of the $-SCH_3$ complexes and can be assigned accordingly. The weak feature observed in the ferrous $Na^+[Fe(S_2$-o-xyl$)_2^{2-}]$ complex is due to detachment of the single Fe $3d$ β electron. The strong D band in both of the bidentate complexes is due to the detachment of the π-electron from the benzene ring in the $=S_2$-o-xyl ligand. A similar band in the same binding energy range was also observed in the PES spectra of $C_6H_5CO_2^-$ and other substituted benzene anions.[44]

The ADEs and Redox Potentials. A one-electron oxidation reaction, aside from solvation effects, is similar to electron detachment in the gas phase. Therefore, the gas phase ADEs should be inherently related to oxidation potentials, except that the solvation effects are absent in the electron detachment in a vacuum. As discussed above, the threshold feature (X) in the PES spectrum of each ferrous complex corresponds to removing a β spin Fe $3d$ electron. This detachment channel represents an oxidation process of Fe(II) → Fe(III). As shown previously,[40] the width of this detachment feature, i.e., the energy difference between the VDE and ADE, directly reflects the geometry changes after one electron is removed, and hence is related to the intrinsic reorganization energy (λ_{ox}) of the Fe^{II}/Fe^{III} redox couple. The VDE and ADE differences of all the complexes are also given in Table 1. Our measured λ_{ox} of $Fe(SCH_3)_3^{1-/0}$ and $Na^+[Fe(S_2$-o-xyl$)_2^{2-/1-}]$ is about 30 kJ/mol, higher than the corresponding value calculated for $Fe(SCH_3)_4^{2-/1-}$ (18.3 kJ/mol, calculated in a vacuum).[45]

The energy gap (ΔE between feature X and A) observed in each ferrous complex is also given in Table 1. Detachment of the Fe $3d$ β electron in each ferrous complex reaches the ground state of the corresponding ferric complexes. Thus, the feature (X) represents the ground state of the ferric complex in each case, whereas all the other PES features represent the excited electronic states of the ferric complex. The spacings of the excited-state features relative to the ground state correspond to the optical excitation energies of the ferric complexes. According to our assignments for the ferrous complexes, the feature (A) is due to electron detachment from the ligand MOs. The ΔE, i.e., the energy spacing between A and X, then represents the ligand-to-metal charge-transfer transition within the ferric complex. The ΔE values for the four ferrous complexes are all around 1 eV (Table 1), which is consistent with previous optical absorption experiments.[14]

Conclusions

Photoelectron spectra of a series of [1Fe] Fe−S complexes, $Fe(SCN)_3^-$, $Fe(SCN)_4^-$, $Na^+[Fe(SCN)_4^{2-}]$, $Fe(SCH_3)_3^-$, $Fe(SCH_3)_4^-$, $Na^+[Fe(S_2$-o-xyl$)_2^{2-}]$, and $Fe(S_2$-o-xyl$)_2^-$, were reported. Detailed electronic structure information about the ferric and ferrous complexes was revealed. For all the ferrous complexes, a weak threshold feature was observed due to detachment of the Fe $3d$ electron that would be transferred in redox reactions involving the Fe^{II}/Fe^{III} couple. Intrinsic redox potentials and the reorganization energies upon oxidation of the ferrous complexes are obtained from the adiabatic and vertical detachment energies of the weak threshold PES feature. By comparing with a $3d^0$ complex $Sc(SCN)_4^-$, we were able to distinguish either ligand-based or Fe $3d$ features. The detachment cross-sections for the Fe $3d$ levels were observed to be very

low within our photon energy range. The spectral patterns of both ferrous and ferric complexes are consistent with the spin-polarized calculations, that give the "inverted level scheme". Our experimental results suggest that the "inverted level scheme" should be a general feature for the high-spin Fe−S complexes regardless of the oxidation state and coordination number. The current results provide an extensive data set that can be used to verify more advanced theoretical calculations for these important and complex electronic systems. Further research is underway to understand in detail the energetics of the redox couple in rubredoxin using the PES data on the $-SCH_3$ complexes.[46]

References and Notes

(1) Lovenberg, W.; Sobel, B. *Proc. Natl. Acad. Sci. U.S.A.* **1965**, *54*, 193.

(2) Eggink, G.; Engel, H.; Vriend, G.; Terpstra, P.; Witholt, B. *J. Mol. Biol.* **1990**, *212*, 135.

(3) Gomes, C. M.; Silva, G.; Oliveira, S.; LeGall, J.; Liu, M. Y.; Xavier, A. V.; Rodrigures-Pousada, C.; Teixeira, M. *J. Mol. Biol.* **1997**, *272*, 22502.

(4) Cammack, R. *Adv. Inorg. Chem.* **1992**, *38*, 281.

(5) Davison, A.; Switkes, E. S. *Inorg. Chem.* **1971**, *10*, 837.

(6) Davison, A.; Reger, D. L. *Inorg. Chem.* **1971**, *10*, 1967.

(7) Anglin, J. R.; Davison, A. *Inorg. Chem.* **1975**, *14*, 234.

(8) Coucouvanis, D.; Holah, D. G.; Hollander, F. J. *Inorg. Chem.* **1975**, *14*, 2657.

(9) Holah, D. G.; Coucouvanis, D. *J. Am. Chem. Soc.* **1975**, *97*, 6917.

(10) Lane, R. W.; Ibers, J. A.; Frankel, R. B.; Holm, R. H. *Proc. Natl. Acad. Sci. U.S.A.* **1975**, *72*, 2868.

(11) Lane, R. W.; Ibers, J. A.; Frankel. R. B.; Papaefthymious, G. C.; Holm, R. H. *J. Am. Chem. Soc.* **1977**, *99*, 84.

(12) Coucouvais, D.; Swenson, D.; Baenziger, N. C.; Murphy, C.; Holah, D. G.; Sfarnas, N.; Simopoulos, A.; Kostikas, A. J. *J. Am. Chem. Soc.* **1981**, *103*, 3350.

(13) Hagen, K. S.; Watson, A. D.; Holm, R. H. *J. Am. Chem. Soc.* **1983**, *105*, 3905.

(14) Gehard, M. S.; Deaton, J. C.; Koch, S. A.; Millar, M.; Solomon, E. I. *J. Am. Chem. Soc.* **1990**, *112*, 2217.

(15) Febhard, M. S.; Koch, S. A.; Millar, M.; Devlin, F. J.; Stephens, P. J.; Solomon, E. I. *J. Am. Chem. Soc.* **1991**, *113*, 1640.

(16) Maelia, L. E.; Millar, M.; Koch, S. A. *Inorg. Chem.* **1992**, *31*, 4594.

(17) Silver, A.; Koch, S. A.; Millar, M. *Inorg. Chim. Acta* **1993**, *205*, 9.

(18) Czernuszewicz, R. S.; Kilpatrick, L. K.; Koch, S. A.; Spiro, T. G. *J. Am. Chem. Soc.* **1994**, *116*, 7134.

(19) Churchill, M. R.; Wormald, J. *Inorg. Chem.* **1975**, *14*, 2657.

(20) Coucouvanis, D.; Swenson, D.; Baenziger, N. C.; Holah, D. G.; Kostikas, A.; Simopoulos, A.; Petrouleas, V. *J. Am. Chem. Soc.* **1976**, *98*, 5721.

(21) Bair, R. A.; Goddard, W. A., III. *J. Am. Chem. Soc.* **1978**, *100*, 5669.

(22) Koerner, J. B.; Ichiye, T. *J. Phys. Chem. B* **1997**, *101*, 3633.

(23) Vaughan, D. J.; Tossell, J. A.; Johnson, K. H. *Geochim. Cosmochim. Acta* **1974**, *38*, 993.

(24) Noman, J. G., Jr.; Jachels, S. C. *J. Am. Chem. Soc.* **1975**, *97*, 3833.

(25) Noodleman, L.; Norman, J. G., Jr.; Osborne, J. H.; Aizman, A.; Case, D. A. *J. Am. Chem. Soc.* **1985**, *107*, 3418.

(26) Noodleman, L.; Case, D. A. *Adv. Inorg. Chem.* **1992**, *38*, 423.

(27) Noodleman, L.; Peng, C. Y.; Case, D. A. Mouesca, J. M. *Coord. Chem. Rev.* **1995**, *144*, 199.

(28) Butcher, K. D.; Gebhard, M. S.; Solomon, E. I. *Inorg. Chem.* **1990**, *29*, 2067.

(29) Rose, K.; Shadle, S. E.; Eidsness, M. K.; Kurtz, D. M., Jr.; Scott, R. A.; Hedman, B.; Hodgson, K. O.; Solomon, E. I. *J. Am. Chem. Soc.* **1998**, *120*, 10743.

(30) Glaser, T.; Hedman, B.; Hodgson, K. O.; Solomon, E. I. *Acc. Chem. Res.* **2000**, *33*, 859.

Electronic Structure of [1Fe] Fe−S Complexes

J. Phys. Chem. A, Vol. 107, No. 11, 2003 **1709**

(31) Howard, J. B.; Rees, D. C. *Chem. Rev.* **1996**, *96*, 2965. Recent X-ray structure suggests that the Fe may be coordinated additionally by a nitrogen atom, which was not revealed in the early study. See Einsle, O.; Tezcan, F. A.; Andrade, S. L. A.; Schmid, B.; Yoshida, M.; Howard, J. B.; Rees, D. C. *Science* **2002**, *297*, 1696.

(32) Lee, H. I.; Hales, B. J.; Hoffman, B. M. *J. Am. Chem. Soc.* **1997**, *119*, 11395.

(33) Yoo, S. J.; Angove, H. C.; Papaefthymiou, V.; Burgess, B. K.; Münck, E. *J. Am. Chem. Soc.* **2000**, *122*, 4926.

(34) MacDonnell, F. M.; Ruhlandt-Senge, K.; Ellison, J. J.; Holm, R. H.; Power, P. P. *Inorg. Chem.* **1995**, *34*, 1815.

(35) Sanakis, Y.; Power, P. P.; Stubna, A.; Münck, E. *Inorg. Chem.* **2002**, *41*, 2690.

(36) Wang, L. S.; Ding, C. F.; Wang, X. B.; Barlow, S. E. *Rev. Sci. Instrum.* **1999**, *70*, 1957.

(37) Wang, L. S.; Wang, X. B. *J. Phys. Chem. A* **2000**, *104*, 1978−1990.

(38) Wang, X. B.; Wang, L. S.; Brown, R.; Schwerdtfeger, P.; Schröder, D.; Schwarz, H. *J. Chem. Phys.* **2001**, *114*, 7388−7395.

(39) Wang, X. B.; Wang, L. S. *J. Phys. Chem. A* **2000**, *104*, 4429.

(40) Wang, X. B.; Wang, L. S. *J. Chem. Phys.* **2000**, *112*, 6959.

(41) Wang, X. B.; Wang, L. S. *J. Am. Chem. Soc.* **2000**, *122*, 2339.

(42) Wang, X. B.; Wang, L. S. *J. Am. Chem. Soc.* **2000**, *122*, 2096.

(43) Noodleman, L.; Norman, J. G., Jr. *J. Chem. Phys.* **1979**, *70*, 4903.

(44) Wang, X. B.; Nicholas, J. B.; Wang, L. S. *J. Chem. Phys.* **2000**, *113*, 653.

(45) Sigfridsson, E.; Olsson, M. H. M.; Ryde, U. *Inorg. Chem.* **2001**, *40*, 2509.

(46) Niu, S. Q.; Wang, X. B.; Nichols, J. A.; Wang, L. S.; Ichiye, T. To be published.